PHYSICAL REVIEW VOLUME 150, NUMBER 1 7 OCTOBER 1966

Electron-Paramagnetic-Resonance Investigation of the Superhyperfine Structure of Iron-Group Impurities in II-VI Compounds*

T. L. ESTLE AND W. C. HOLTON
Texas Instruments, Inc., Dallas, Texas

(Received 14 May 1966)

The electron-paramagnetic-resonance spectra of several iron-group impurities in ZnSe, ZnTe, and CdTe are shown to have resolved superhyperfine structure (SHFS) resulting from an interaction with one or two shells of Se or Te nuclei surrounding the impurity. We have observed interaction with the two nearest chalcogenide shells for ZnSe:Cr$^+$, ZnSe:Mn^{2+}, ZnTe:Cr$^+$, ZnTe:Mn^{2+}, and ZnTe:Fe$^+$, and an interaction with only the nearest chalcogenide shell for ZnSe:Fe^{3+}, ZnSe:Cr^{2+}, and CdTe:Mn^{2+}. Hensel's data on Fe^{3+} in ZnTe were analyzed for the first-shell Te SHFS. None of these data exhibit Zn^{67} SHFS, although the Cd chalcogenides show Cd SHFS. Several other impurities in II-VI compounds were studied to obtain additional information on SHFS. The SHFS results are compared for different impurities and crystals and discussed in relation to the delocalization expected from covalent bonding. The small observed delocalization is surprising in view of the fairly large covalent character of the crystals.

I. INTRODUCTION

ONE of the characteristics of iron-transition-group ions resulting from their incorporation as impurities into crystalline environments is the resultant delocalization of the electronic orbitals. This delocalization leads to hyperfine interactions with nuclei neighboring the impurity which are much larger than calculated for point-dipole interactions. These interactions with nearby nuclei and the resultant superhyperfine structure (SHFS) in the electron paramagnetic resonance (EPR) spectrum of the impurity ion will be the principal subject of this paper.

The first observation of SHFS was made by Owen and Stevens,[1] who studied the EPR of Ir, a platinum-group impurity, in ammonium chloroplatinate. They attributed the observed SHFS to an interaction resulting from the effects of covalent bonding. Tinkham[2] demonstrated the same behavior for iron-group impurities in ZnF$_2$ and laid the basis for most subsequent investigations of the subject. In these and most of the later studies,[3] the host crystals were primarily ionic. However, the small covalent bonding present even in ionic crystals dominates the SHFS. Although complicated, the theoretical analyses[4] of this problem show considerable promise for ionic crystals.

Since covalent bonding is responsible for SHFS, it is of interest to explore the characteristics of iron-group impurities in crystals which are more covalent. Dorain[5] was the first to report SHFS of iron-group impurities in fairly covalent crystals. He observed Cd SHFS for Mn^{2+} impurities in CdS. Subsequently, a number of EPR observations of SHFS of iron-group impurities in II-VI compounds were made. Cadmium SHFS was observed for Mn^{2+} in CdSe[6] and CdTe,[7,8] for Cr$^+$ in CdTe,[9] for V^{3+} in CdS,[10] for Cr^{2+} in CdS,[11] and for Co^{2+} in CdS.[12] Zinc SHFS was observed for Cr$^+$ in ZnS,[13] and for Mn^{2+} in ZnS.[6] In addition to these observations, Title[14] observed SHFS for Cr$^+$ in ZnSe and ZnTe. The interpretation of Title's results will be dealt with later in this paper. After the completion of the major part of this work,[15] we learned that observations similar to ours were made for Fe^{3+} in ZnTe by Hensel[16] and for Fe^{3+} in ZnSe by Dieleman.[17]

The II-VI compounds which are of interest in this discussion because of their covalent character are the zinc and cadmium chalcogenides. Except for CdO, these compounds normally have the zinc blende or Wurtzite structure, both of which are four-coordinated structures and possess rather similar properties for our present purposes. In the zincblende structure, shown in Fig. 1, the neighbors of a substitutional metal site consist of a first shell of four chalcogenides, a second shell of 12 metal ions, and a third shell of 12 chalcogenides. In the absence of distortions resulting from replacing the host metal ion by the impurity, the relative distances of the first three shells from the impurity site are 1, 1.632, and 1.918. The observations mentioned in the previous

---

* This work was supported in part by U. S. Air Force Office of Scientific Research Contract No. AF 49(638)-1250.

[1] J. Owen and K. W. H. Stevens, Nature **171**, 836 (1953).

[2] M. Tinkham, Proc. Roy. Soc. (London) **A236**, 535 (1956); **A236**, 549 (1956).

[3] See, for example, T. P. P. Hall, W. Hayes, R. W. H. Stevenson, and J. Wilkens, J. Chem. Phys. **38**, 1977 (1963); **39**, 35 (1963), and references cited therein.

[4] S. Sugano and Y. Tanabe, J. Phys. Soc. Japan **20**, 1155 (1965); E. Simánek and Z. Sroubek, Phys. Status Solidi **4**, 251 (1964); R. E. Watson and A. J. Freeman, Phys. Rev. **134**, A1526 (1964).

[5] P. B. Dorain, Phys. Rev. **112**, 1058 (1958).

[6] J. Schneider, S. R. Sircar, and A. Räuber, Z. Naturforsch. **18a** 980 (1963).

[7] J. Lambe and C. Kikuchi, Phys. Rev. **119**, 1256 (1960).

[8] T. P. P. Hall, W. Hayes, and F. I. B. Williams, Proc. Phys. Soc. **78**, 883 (1961).

[9] G. W. Ludwig and M. R. Lorenz, Phys. Rev. **131**, 601 (1963).

[10] G. W. Ludwig and H. H. Woodbury, in *Solid State Physics*, edited by F. Seitz and D. Turnbull (Academic Press Inc., New York, 1962), Vol. 13, p. 299.

[11] T. L. Estle, G. K. Walters, and M. de Wit, in *Paramagnetic Resonance*, edited by W. Low (Academic Press Inc., New York, 1963), Vol. 1, p. 144.

[12] R. E. De Kinder, Jr., Bull. Am. Phys. Soc. **10**, 173 (1965).

[13] J. Dieleman, R. S. Title, and W. V. Smith, Phys. Letters **1**, 334 (1962).

[14] R. S. Title, Phys. Rev. **133**, A1613 (1964).

[15] T. L. Estle and W. C. Holton, Bull. Am. Phys. Soc. **10**, 57 (1965).

[16] J. C. Hensel, Bull. Am. Phys. Soc. **9**, 244 (1964).

[17] J. Dieleman, Phillips Res. Repts. **20**, 206 (1965).

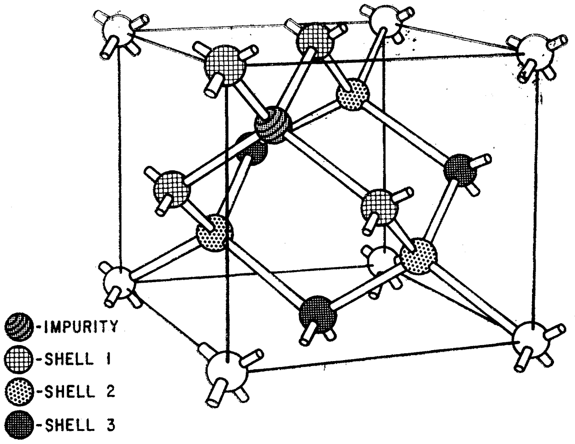

FIG. 1. Neighbors of an impurity in the zinc-blende structure. The first shell of neighbors of a metallic impurity are four chalcogenide ions situated along ⟨111⟩ tetrahedral bond axes. The second shell consists of 12 metal ions which are along ⟨110⟩ axes in the absence of distortion. Similarly, the third shell consists of 12 chalcogenides which for no distortion are situated along ⟨311⟩ crystal axes.

paragraph, except for the Fe^{3+} results,[16,17] were interpreted in terms of an interaction with the nearest shell of metal ions, which is the second shell of neighbors and is about 60% further from the impurity than the first shell. On this basis the apparent absence of SHFS arising from the first shell was unexpected. Because of the low relative abundance of the isotopes of oxygen and sulfur which have nonzero nuclear spin, ZnO and ZnS are not well suited to the observation of chalcogenide SHFS. Similarly, because of the high relative abundance of isotopes of Cd with a nuclear spin of $\frac{1}{2}$, the Cd chalcogenides are not suitable. However, ZnSe and ZnTe do provide a good opportunity to observe Se or Te SHFS because of the low relative abundance of Zn isotopes with a nuclear moment and the moderate abundance of Se and Te isotopes with a nuclear moment. This is clarified in Table I, which shows the relative intensities of the superhyperfine lines to be expected from a given number of equivalent nuclei of the pertinent Column II and Column VI elements.

We have examined the EPR spectra of several iron-group impurities in ZnSe and ZnTe. SHFS is observed for Cr^+, Mn^{2+}, Fe^{3+}, and Cr^{2+} in ZnSe and Cr^+, Mn^{2+}, and Fe^+ in ZnTe. These data are explained by the chalcogenide SHFS, which had remained unobserved until recently, but which is just as promiment as metal ion SHFS in II-VI compounds. For the zinc chalcogenides, the first-shell interaction was observed in all seven cases; five cases (Fe^{3+} and Cr^{2+} excepted) showed resolved SHFS arising from the third shell, which also consists of chalcogenides. The existence of a second-shell Zn^{67} interaction was not apparent in any of the data. Other characteristics of the data are discussed in Sec. V of this paper.

In addition to the observations for impurities in ZnSe and ZnTe, we have studied Mn^{2+} in CdTe, Fe^{3+} in CdS, and Cr^+ in ZnS. We have also examined the spectra of Cr^+ in CdTe published by Ludwig and Lorenz.[9] These data allow us to give an approximate value for the Te^{125} SHFS constant for Mn^{2+} in CdTe and an upper limit for the following: (1) the Cd SHFS constant for Fe^{3+} in CdS, (2) the S^{33} SHFS constant for Cr^+ in ZnS, and (3) the Te^{125} SHFS constant for Cr^+ in CdTe. Finally, we have augmented the information on SHFS by analyzing data obtained by Hensel on Fe^{3+} in ZnTe.

In addition to the information obtained concerning SHFS, other characteristics of the EPR data will be discussed for the isoelectronic *S*-state ions Cr^+, Mn^{2+}, and Fe^{3+} in ZnSe and ZnTe. Since the Fe^+ and Cr^{2+} results will be discussed further in subsequent publications, these data will receive only limited examination here. Besides confirming the values of several spin-Hamiltonian parameters reported by others, we have determined the sign of the cubic crystalline field parameter for Cr^+ in ZnTe, observed cross terms between the hyperfine interaction and the cubic field splitting for Mn^{2+} in ZnSe, and determined the properties of Cr^{2+} in ZnSe and Fe^+ in ZnTe.

Numerous prior EPR investigations of ZnSe and ZnTe have been reported. Title[14] has studied Cr^+ in ZnSe and ZnTe, Hensel[16] has studied Fe^{3+} in ZnTe, and Dieleman[17]

TABLE I. Isotopes with nonzero nuclear spin for pertinent Column II and Column VI elements and their expected SHFS intensity patterns for natural abundance.

Isotope	Relative abundance (%)	Nuclear spin	Relative intensities for 4 equivalent nuclei	Relative intensities for 12 equivalent nuclei
Zn^{67}	4.12	$\frac{5}{2}$		1.000, 0.086, 0.017, 0.086, 0.013, 0.086, 0.010, 0.001, 0.007, 0.001, 0.003
Cd^{111}	12.86	$\frac{1}{2}$		1.000, 0.839, 0.501, 0.218, 0.071, 0.017, 0.003
Cd^{113}	12.34	$\frac{1}{2}$		
O^{17}	0.037	$\frac{5}{2}$	1.000	1.000, 0.001, 0.000, 0.001, 0.000, 0.001
S^{33}	0.74	$\frac{3}{2}$	1.000, 0.007, 0.000, 0.007	1.000, 0.022, 0.001, 0.022
Se^{77}	7.50	$\frac{1}{2}$	1.000, 0.160, 0.010	1.000, 0.434, 0.093, 0.012, 0.001
Te^{123}	0.89	$\frac{1}{2}$	1.000, 0.169, 0.011	1.000, 0.454, 0.130, 0.014, 0.001
Te^{125}	7.03	$\frac{1}{2}$		

has studied Fe^{3+} in ZnSe. Several investigators have studied Mn^{2+} in ZnSe[18] and ZnTe.[19] Co^{2+} has been studied in ZnSe and ZnTe,[20] and centers produced in V- and Cr-doped ZnTe have been reported.[21]

The remainder of the paper is divided into four major sections. Section II contains a brief discussion of the experimental and computational techniques employed in this study. The required spin-Hamiltonian descriptions are given in Sec. III. In Sec. IV the results are presented and analyzed in terms of the appropriate spin-Hamiltonian, and in Sec. V the SHFS results are discussed.

II. EXPERIMENTAL AND COMPUTATIONAL PROCEDURE

The superheterodyne EPR spectrometer used in this investigation operated near 9.2 GHz. The samples were maintained at 1.3°K during study and irradiated with monochromatic light when desired. Orientation of the samples was obtained either from cleavage faces of the crystals or from an x-ray-diffraction analysis. Accurate alignment of any particular crystalline direction along the magnetic field was obtained by mounting the crystal on a rotating table in the microwave cavity, rotating the table about a horizontal axis and the magnet about a vertical axis. The samples were prepared by diffusing the desired impurity from an evaporated metal layer into nominally-pure crystals. Some spectra were also observed in the nominally pure crystals.

In order to make careful comparisons between the observed spectra and the spectra expected for a particular explanation of the superhyperfine interaction, a computer program was developed to construct superhyperfine spectra. The program calculates the shape of the spectrum expected for the symmetric hyperfine pattern resulting from identical Gaussian lines generated by several shells of nuclear moments. Each shell may contain up to three isotopes with different nuclear spins and moments. The experimentally observed spectra were compared with the spectra derived by the computer with various assumptions as to splittings and explanations for the structure.

III. SPIN-HAMILTONIAN DESCRIPTION

Iron transition-group impurities in ZnSe, ZnTe, and CdTe are found to incorporate substitutionally for the metal ion, which is at a site of tetrahedral symmetry. As shown in Fig. 1, the closest shell of nuclei consists of four chalcogenide ions situated along the $\langle 111\rangle$ crystal axes. The second shell of neighbors consists of 12 metal ions situated along $\langle 110\rangle$ crystal axes in the absence of distortions, and the third shell of neighbors consists of 12 chalcogenide ions situated along $\langle 311\rangle$ crystal axes, also assuming no distortion.

The appropriate spin-Hamiltonian for a $3d^5$ S-state impurity ion (Fe^{3+}, Mn^{2+}, Cr^{+}) in tetrahedral symmetry is

$$\mathcal{H}=g\beta\mathbf{H}\cdot\mathbf{S}+\tfrac{1}{6}a\{S_x^4+S_y^4+S_z^4-\tfrac{1}{5}S(S+1)(3S^2+3S-1)\}+\mathcal{H}_{hf}, \qquad (1)$$

where

$$\mathcal{H}_{hf}=A\mathbf{I}\cdot\mathbf{S}+\textstyle\sum_n \{\mathbf{S}\cdot\mathbf{A}_n\cdot\mathbf{I}_n+g_n\beta_n\mathbf{H}\cdot\mathbf{I}_n\}, \qquad (2)$$

where the sum over n is taken over all nuclei having an appreciable interaction with the impurity spin. In Eq. (1), the first term is the electronic Zeeman interaction, the second is the cubic field term, and the third is the hyperfine interaction. In Eq. (2), the first term is the hyperfine interaction with the impurity nucleus, the second is the superhyperfine interaction with lattice nuclei, and the last term is the nuclear Zeeman interaction. The cubic axes of the crystal are denoted by x, y, and z and the spin S is $\frac{5}{2}$.

The characteristics of Fe^{+} in tetrahedral symmetry are similar to those of isoelectronic Co^{2+} described by Ham, Ludwig, Watkins, and Woodbury.[20] The appropriate spin-Hamiltonian for $Fe^{+}(3d^7)$ in T_d symmetry is

$$\mathcal{H}=g\beta\mathbf{H}\cdot\mathbf{S}+u\beta\{S_x^3H_x+S_y^3H_y+S_z^3H_z-\mathbf{S}\cdot\mathbf{H}[3S(S+1)-1]\}. \qquad (3)$$

The second term has been shown by Bleaney[22] and Koster and Statz[23] to be allowed by symmetry. The cubic axes of the crystal are denoted by x, y, and z and the spin S is $\frac{3}{2}$.

In the tetrahedrally symmetric substitutional site in ZnSe, the Cr^{2+} ion undergoes a spontaneous distortion along $\langle 100\rangle$ axes as a result of the Jahn-Teller effect.[24] This is also observed for Cr^{2+} in CdS.[11] The lowest levels result from an orbital singlet with spin equal two. The observed transitions are between the $M=2$ and $M=-2$ states and can be described in terms of an effective spin-Hamiltonian of the form[11]

$$\mathcal{H}=g_{\|}'\beta H_zS_z'+\Delta S_x'+\mathcal{H}_{hf}', \qquad (4)$$

where the effective spin S' is $\frac{1}{2}$. Since the effective spin (and the real spin) are fixed in direction, only the g value and hyperfine constants for this direction are measureable. The hyperfine splittings cannot be expressed in energy units since the actual g factor must be known to make such a conversion. Since the actual g factor appears to be close to two, the values in cm^{-1} are approximately those in gauss times 10^{-4}.

---

[18] R. S. Title, Phys. Rev. **131**, 2503 (1963); B. C. Cavenett, Proc. Phys. Soc. **84**, 1 (1964).

[19] C. Kikuchi and G. H. Azarbayejani, J. Phys. Soc. Japan **17**, Suppl. B-I, 453 (1962); S. Kunii and E. Hirahara, *ibid.* **19**, 1258 (1964).

[20] F. S. Ham, G. W. Ludwig, G. D. Watkins, and H. H. Woodbury, Phys. Rev. Letters **5**, 468 (1960).

[21] See Ref. 10, p. 298.

[22] B. Bleaney, Proc. Roy. Soc. (London) **A73**, 939 (1959).

[23] G. F. Koster and H. Statz, Phys. Rev. **113**, 445 (1959).

[24] M. de Wit, A. R. Reinberg, W. C. Holton, and T. L. Estle, Bull. Am. Phys. Soc. **10**, 329 (1965).

IV. RESULTS

A. ZnSe:Cr$^+$

Single crystals of ZnSe doped with chromium show a strong Cr$^+$ EPR spectrum, as shown in Figs. 2 and 3. The spectrum is enhanced by irradiating the crystal at 1.3°K with 2.9-eV light. Frequently, crystals which were not intentionally doped with chromium also show the Cr$^+$ EPR spectrum after optical excitation. The spectrum with the magnetic field along a $\langle 100\rangle$ crystal axis is identical to that observed by Title[14] except that the fine structure is not observed in our crystal, presumably because of strain broadening. In agreement with Title, we find [see Eqs. (1) and (2)] $g=2.0018\pm0.0005$ and $A_{\mathrm{Cr}^{53}}=(13.27\pm0.04)\times10^{-4}$ cm^{-1}. The fine-structure constant was determined by Title from the observed fine structure to be $a=(5.35\pm0.08)\times10^{-4}$ cm^{-1}.

We have interpreted the SHFS as arising from the first and third shells of neighboring nuclei. This interpretation differs from that of Title,[14] who attributes the SHFS to the second shell, the zinc neighbors. Thus, we have made a very careful comparison of all of the characteristics expected from our interpretation and from Title's interpretation, both with our experimental data and with Title's spectrum from Fig. 1 of his paper.[14] In Fig. 3 we have compared the spectrum observed with the magnetic field along a $\langle 100\rangle$ axis to a spectrum constructed by the computer. The ratios of the three hyperfine splittings and the linewidth were chosen for the best agreement with the experimental data, but no other parameters were adjusted. The correspondence of the constructed spectrum with our experimental spectrum is excellent. Rather good correspondence with Title's published spectrum[14] is also achieved, except for the differences produced by the fine structure. Attempts to reproduce the observed spectrum by employing an isotropic Zn^{67} hyperfine interaction but no Zn^{67} quadrupole interaction either with or without a selenium interaction gave results in conflict with the observations. On this basis it appears that any hyperfine splitting produced by second-shell zinc ions is probably less than 0.1×10^{-4} cm^{-1}. Additional support for our interpretation is given by the angular dependence of the SHFS. The SHFS pattern near the line which is third from the center on either side arises from the first shell in our interpretation. The observed positions of the lines shown in Fig. 2 fit precisely with that expected from four nuclei along $\langle 111\rangle$ axes. The results for data taken along $\langle 001\rangle$, $\langle 111\rangle$, $\langle 110\rangle$, and $\langle 112\rangle$ can be explained by an axial superhyperfine interaction with principal values of $|A_1|=(6.83\pm0.04)\times10^{-4}$ cm^{-1} and $|B_1|=(4.41\pm0.03)\times10^{-4}$ cm^{-1}. Since the remaining seven cases we have studied, consisting of both selenides and tellurides, can also be explained on the basis of an interaction with the first two chalcogenide shells, and since there is excellent agreement between the computed and experimental spectra for all crystal orientations studied, we believe that our explanation is correct. The remainder of this paper will therefore treat this as an established fact. Observation of the angular variation of the third-shell structure showed only slight variations in the positions and intensities of the lines. For no orientation of the crystal in the magnetic field are all third-shell selenium ions

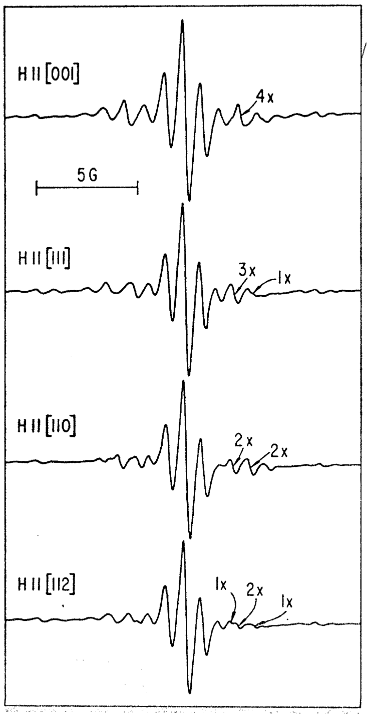

FIG. 2. The observed EPR spectra for Cr$^+$ in ZnSe at 1.3°K and 9.16 GHz. The magnetic field is oriented along the four crystalline axes which produce the simplest spectra. The number of identical first-shell nuclei contributing to the most prominent lines of the first-shell SHFS are indicated.

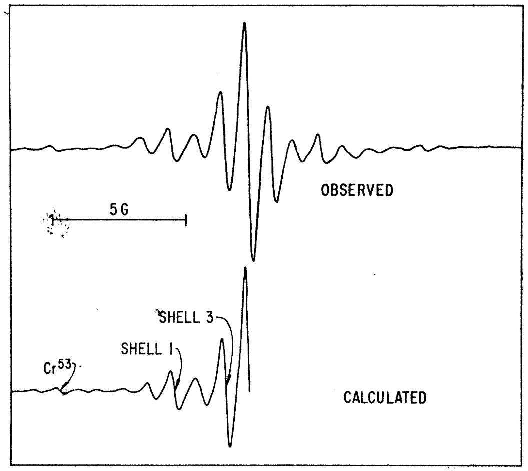

FIG. 3. The observed and calculated EPR spectrum for Cr$^+$ in ZnSe at 1.3°K and 9.16 GHz with the magnetic field along a $\langle 100\rangle$ axis. The calculated spectrum was obtained by placing Gaussian-shaped lines at all positions predicted for an interaction with Se^{77} nuclei in shells 1 and 3. The splittings were chosen to give the best fit to the experimental data and are in the ratio $A_1{:}A_3{:}A_{\mathrm{Cr}^{53}}{:}\Delta H=1{:}0.309{:}2.52{:}0.057$.

magnetically equivalent, although the nonequivalent ions could not be resolved experimentally. Thus the measured splitting represents only an average value for the observed superhyperfine splitting,

$$|\bar{A}_3| = (1.65\pm0.02)\times10^{-4}\ \mathrm{cm}^{-1}.$$

The Zeeman interaction of nuclei with the applied magnetic field given by the last term in $\mathcal{H}_{hf}$ [see Eq. (2)] can usually be ignored in describing the hyperfine splittings observed in EPR. However, if it is comparable in magnitude to the hyperfine interaction and if the latter is rather anisotropic, then the direction of the local magnetic field at the nucleus will be influenced and the observed splittings will be affected. Such a situation could arise for ZnSe:Cr^+. Experimentally, the third-shell interaction does not provide a sufficient amount of information to disentangle the two interactions. However, for the first-shell interaction, a deviation of the predicted angular dependence by an amount only slightly greater than the experimental error is expected if A_1 and B_1 differ in sign, but an unobservable effect if they have the same sign. No effect was observed, which would suggest that A_1 and B_1 have the same sign. Because of the small size of the expected effect, no great confidence can be attached to this observation. Therefore, both first- and third-shell hyperfine interactions are uncertain to the extent that the nuclear Zeeman interaction has not been included.

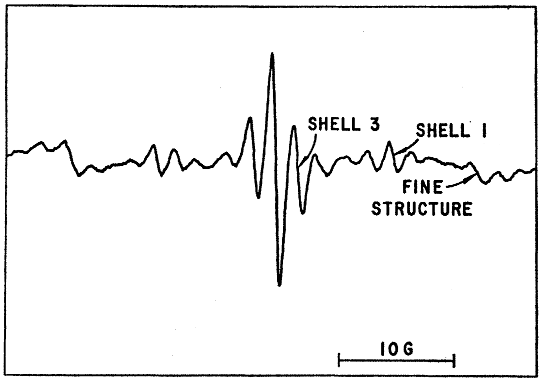

FIG. 4. The observed EPR spectrum for Cr^+ in ZnTe at 1.3°K and 9.16 GHz with the magnetic field along a ⟨100⟩ axis. The spectrum is qualitatively similar to that for Cr^+ in ZnSe except for the presence of the fine structure.

B. ZnTe:Cr^+

The results for Cr^+ in ZnTe, as shown in Fig. 4, are quite similar to those for Cr^+ in ZnSe. This is because the isotopic abundances of Se^{77} and Te^{125} are similar and both have a spin of $\frac{1}{2}$. The main difference is that the fine structure was observed for our ZnTe:Cr^+ sample but not for our ZnSe:Cr^+ sample. In agreement with Title,[14] we find the spin-Hamiltonian parameters [see Eq. (1)] to be $g=2.0026\pm0.0005$, $|A_{\mathrm{Cr}^{53}}| = (12.43\pm0.03)\times10^{-4}\ \mathrm{cm}^{-1}$, and $a=+(6.59\pm0.01)\times10^{-4}\ \mathrm{cm}^{-1}$. The sign of a was determined from relative-intensity measurements at 1.3°K. The first-shell tellurium interaction is described by $|A_1| = (11.8\pm0.2)\times10^{-4}\ \mathrm{cm}^{-1}$ and $|B_1| = (21.83\pm0.02)\times10^{-4}\ \mathrm{cm}^{-1}$. The average value of the third-shell interaction is $|\bar{A}_3| = (3.54\pm0.04)\times10^{-4}\ \mathrm{cm}^{-1}$. The third-shell splittings and intensities suggest a somewhat larger anisotropy than observed for ZnSe:Cr^+. The uncertainties in the experimental data preclude determination of nuclear Zeeman effects for either shell; hence, no such correction is included. The Cr^+ signal in ZnTe is also photosensitive and is enhanced by 2.25-eV light.

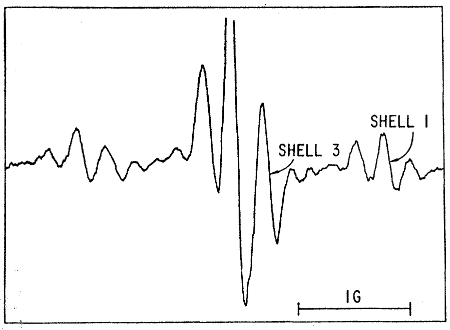

FIG. 5. Part of the observed EPR spectrum for Mn^{2+} in ZnSe at 1.3°K and 9.16 GHz with the magnetic field along a ⟨100⟩ axis. Note particularly the small field region involved. Identical spectra were obtained for the other five Mn^{55} hyperfine lines.

C. ZnSe:Mn^{2+}

EPR was observed for the $M_s=\frac{1}{2}\leftrightarrow-\frac{1}{2}$ transition for all six Mn^{55} hyperfine lines with the magnetic field along the ⟨100⟩ and ⟨111⟩ crystal axes. Several Mn^{55} hyperfine lines were also examined for the field along the ⟨110⟩ and ⟨112⟩ crystal axes. The observed spectrum for one of the Mn^{55} hyperfine lines with the field along a ⟨100⟩ crystal axis is shown in Fig. 5. The results are qualitatively similar to the Cr^+ results.

The spin-Hamiltonian parameters [see Eq. (1)] are $g=2.0057\pm0.0005$ and $A_{\mathrm{Mn}^{55}}=(-61.77\pm0.02)\times10^{-4}\ \mathrm{cm}^{-1}$, in good agreement with earlier observations.[18] Because of the precision with which these measurements could be made, an angular anisotropy of the $M_s=\frac{1}{2}\leftrightarrow-\frac{1}{2}$ transitions was observed. This arises because of cross terms between the cubic crystalline field splitting and the impurity hyperfine interaction. A calculation of the expected anisotropy using third-order perturbation theory gives reasonable agreement with the observed anisotropy, which is about two parts per thousand.

The first- and third-shell superhyperfine interactions were again observed and are described by $|A_1| = (2.10\pm0.08\times10^{-4}\ \mathrm{cm}^{-1}$, $|B_1| = (2.81\pm0.02(\times10^{-4}\ \mathrm{cm}^{-1}$, and $|\bar{A}_3| = (0.44\pm0.03)\times10^{-4}\ \mathrm{cm}^{-1}$. The anisotropy of the third-shell splittings and intensities is much larger than for the previous Cr^+ observations.

In fact, the anisotropy was so great that third-shell structure was unresolved except for the magnetic field direction almost along either the ⟨100⟩ or ⟨111⟩ crystal axes. The lack of a field dependence in the Se^{77} structure, the observation of which was made possible because of the six Mn^{2+} hyperfine lines, suggests that the nuclear Zeeman interaction is small so that A_1 and B_1 have the same sign. This is a tenuous observation, since the effect should have exceeded the experimental uncertainty by less than a factor of two. No effect on the third-shell interaction could have been observed, and none of the data has been so adjusted. The Mn^{2+} resonance was not photosensitive.

D. ZnTe:Mn^{2+}

The EPR results for ZnTe:Mn^{2+} were quite similar to ZnSe:Mn^{2+}. Figure 6 shows the spectra that were observed with the magnetic field along the ⟨100⟩ and ⟨111⟩ crystal axes. A large third-shell anisotropy is evident in these results. This anisotropy is greater than that for Cr^+ in ZnSe or ZnTe but less than that for Mn^{2+} in ZnSe. The superhyperfine constants are $|A_1| = (3.21\pm0.15)\times10^{-4}$ cm^{-1}, $|B_1| = (4.85\pm0.07)\times10^{-4}$ cm^{-1}, and $|\bar{A}_3| = (1.14\pm0.03)\times10^{-4}$ cm^{-1}. The Mn^{2+} signal in ZnTe was not photosensitive.

E. CdTe:Mn^{2+}

A study of the SHFS of the highest and lowest field $M_s = \frac{1}{2} \leftrightarrow -\frac{1}{2}$ lines for Mn^{2+} in CdTe with the magnetic field along a ⟨111⟩ crystal axis shows characteristics which can be explained in terms of Te^{125} SHFS. The regularly spaced pattern resulting from Cd^{111} and Cd^{113} SHFS[7,8] is interrupted after the third line from the center of the Cd SHFS pattern. This characteristic is consistent with a Te^{125} hyperfine interaction constant of the order of 10×10^{-4} cm^{-1}. No further quantitative analysis of this spectrum appears possible. Other Mn^{2+} hyperfine lines or other orientations of the crystal in the magnetic field were not suitable for observing the Te^{125} interaction. As in the case of ZnSe and ZnTe, this EPR signal was not influenced by light.

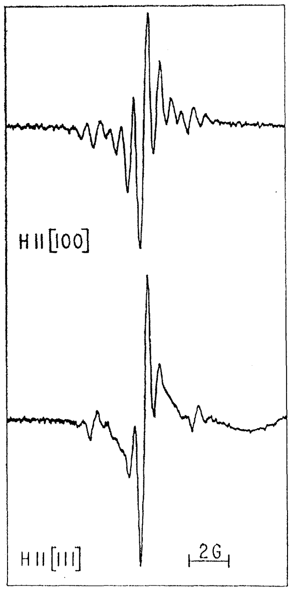

FIG. 6. Part of the observed EPR spectrum for Mn^{2+} in ZnTe at 1.3°K and 9.16 GHz with the magnetic field in two different directions. Identical spectra were obtained for the other five Mn^{55} hyperfine lines. The anisotropy of the third-shell interaction is evident by the loss of resolution (compare with Fig. 2).

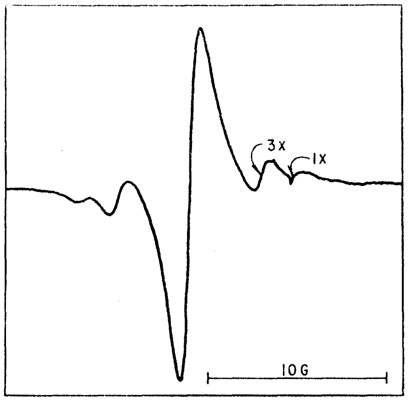

FIG. 7. The observed EPR spectrum for Fe^{3+} in ZnSe at 1.3°K and 9.16 GHz with the magnetic field along the $[111]_w$ axis. The number of identical nuclei contributing to each component of the SHFS is indicated. Note the absence of resolved third-shell structure and the large linewidths as compared to Cr^+ and Mn^{2+}.

F. ZnSe:Fe^{3+}

The EPR spectra for ZnSe:Fe^{3+} (see Fig. 7) differ from those for Cr^+ and Mn^{2+} in that only the first-shell SHFS is resolved. In addition, no fine structure was observed in our crystals, which were macroscopic rotational twins. The spin-Hamiltonian parameters are $g = 2.0470\pm0.0005$, $|a| = (45\pm20)\times10^{-4}$ cm^{-1}, and $|A_{Fe^{57}}| = (6.6\pm0.1)\times10^{-4}$ cm^{-1}. The magnitude of a was obtained from the anisotropy of the observed $M_s = \frac{1}{2} \leftrightarrow -\frac{1}{2}$ transition. The lack of observed fine structure prevented determination of the sign, and of a more precise value of a. The Fe^{57} hyperfine splitting was obtained by using a sample enriched in Fe^{57}. The superhyperfine structure is described by $|A_1| = (11.37\pm0.08)\times10^{-4}$ cm^{-1} and $|B_1| = (7.14\pm0.10)\times10^{-4}$ cm^{-1} for the first shell and $|\bar{A}_3| \lesssim 2.4\times10^{-4}$ cm^{-1} for the third shell of neighbors. The Fe^{3+} signal is photosensitive and can be generated by 2.9-eV light. These results are in good agreement with those of Dieleman,[17] although his values are more precise since his unstrained crystals allowed him to observe the fine structure and to obtain better resolution.

G. ZnTe:Fe^{3+}

The SHFS for ZnTe:Fe^{3+} has been observed by J. C. Hensel and is reported here for the first time.[16,25] For the $M_s = \frac{1}{2} \leftrightarrow -\frac{1}{2}$ transition with the magnetic

---

[25] The results for Fe^{3+} in ZnTe were obtained from data taken especially for this purpose by J. C. Hensel, whose gracious assistance we acknowledge.

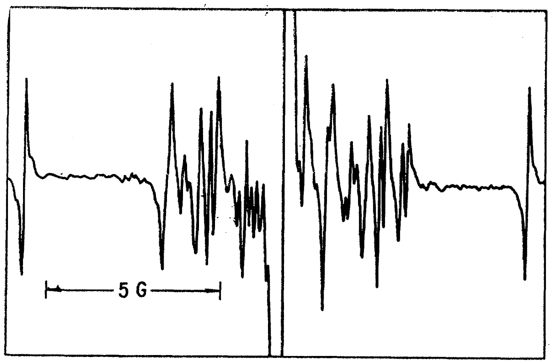

FIG. 8. The observed EPR spectrum for Cr^+ in ZnS at 1.3°K and 9.16 GHz with the magnetic field along the $[111]_w$ axis. The central line is over ten times full scale. The lines at the two extremes of the spectrum are the innermost Cr^{53} hyperfine lines. The small undulations between the Cr^{53} lines and the comparable-intensity SHFS is the SHFS of the Cr^{53} hyperfine lines. Note the extreme narrowness of the lines and the absence of any regularity to the pattern.

field parallel to a $\langle 111\rangle$ crystal axis, only SHFS from the first Te shell is resolved, because of the 7-G linewidth. The superhyperfine constants for Te^{125} in $ZnTe{:}Fe^{3+}$ obtained from Hensel's data are $|A_1| = 22\times10^{-4}$ cm^{-1} and $|B_1| = 16\times10^{-4}$ cm^{-1}.

H. ZnTe:Fe^+

An analysis of the Fe^+ EPR data using the spin-Hamiltonian [see Eq. (3)] appropriate for a $3d^7$ ion in tetrahedral symmetry yields the parameters $g = 2.280$, $u = 5.67\times10^{-3}$, $|A_1| = (3.90\pm0.05)\times10^{-4}$ cm^{-1} for $\mathbf{H}\|[100]$, and $|\tilde{A}_3| = (1.31\pm0.05)\times10^{-4}$ cm^{-1}. The Fe^+ signal is photosensitive and is enhanced by 2.25-eV light. A more detailed description of this system will appear in a future publication.

I. ZnSe:Cr^{2+}

The Cr^{2+} EPR in ZnSe[24] is quite similar to that observed in CdS by Estle, Walters, and de Wit.[11] The effective spin-Hamiltonian of Eq. (4) is used to analyze the data and leads to the parameters $g_{\|}' = 7.837$, $\Delta = 0.72$ GHz, $A_{Cr^{53}}/g\beta = 12.6$ G, and $A_{Se}/g\beta = 4.31$ G. Both the Cr^+ and Cr^{2+} charge state were observed simultaneously in one sample. The optically induced transfer of charge was monitored by observing the decrease of the Cr^{2+} signal as the Cr^+ signal increased. The Cr^+ was created by the trapping of electrons at Cr^{2+} after electron-hole pairs were produced by 2.9-eV light. The center which trapped the hole is not known.

J. ZnS:Cr^+

An examination under conditions of high sensitivity and high resolution has been made of the SHFS of Cr^+ in ZnS, first reported by Dieleman, *et al.*[13] Although the published spectra[13,14,26] appear to consist of six uniformly spaced lines, our observations (shown in Fig. 8) have disclosed at least 30 lines with a very nonuniform spacing and intensity. These spectra were obtained with the magnetic field along the $[111]_w$ axis, i.e., the $\langle 111\rangle$ axis common to the two twinned regions in the rotationally twinned crystal. For other directions the complexity is comparable, which suggests that resolution is limiting the number of lines seen. The spectrum is both asymmetric and anisotropic. The complexity prevented a detailed analysis, but certain conclusions can be drawn. From the asymmetry, anisotropy, and intensity of the lines it appears that a Zn^{67} quadrupole interaction of the order of 10^{-4} cm^{-1} is present. The Zn^{67} hyperfine interaction is about 1.3×10^{-4} cm^{-1}, but cannot be shown to be isotropic. Although the signal-to-noise is adequate to see the S^{33} SHFS lines in good intensity, none could be identified. This allows an upper limit of 2.2×10^{-4} cm^{-1} to be placed on the S^{33} hyperfine constant.

K. Miscellaneous

In addition to the data mentioned above, we have also established upper limits to the first-shell Te interaction for Cr^+ in CdTe by examining the data of Ludwig and Lorenz.[9] This value is $|A_1| \lesssim 10\times10^{-4}$ cm^{-1}. Also, we have examined Fe^{3+} in CdS and have placed an upper limit on the Cd interaction of $|A_2| \lesssim 1.5\times10^{-4}$ cm^{-1}.

V. DISCUSSION

If the various observed hyperfine interactions, summarized in Tables II and III, are attributed to $n = 4$ electrons for Zn and Se and to $n = 5$ electrons for Cd and Te, then the total s and p electron density on all of the neighbors showing appreciable interaction is only a few percent for all cases studied. This rather low value is in fact comparable to the electron densities deduced for transition-group impurities in ionic fluoride crystals.[3] The small extent of the delocalization implied by this estimate is surprising in view of the covalent character of the crystals, and in view of the observed indications of covalent bonding of iron-group impurities in the II-VI compounds as measured by impurity hyperfine constants, g values, and zero-field splittings of S-state ions. Our estimates have been based on values of the principal quantum number corresponding to the last filled shell for the nonmetal and to the lowest unfilled shell for the metal. If the nature of the wave function near a lattice site is more like that of an ionic function of higher n value, then our estimates of the fraction of the wave function localized on the neighbors would be low.

Other features of interest appear upon a detailed comparison of the results for the various cases studied by us and by earlier workers, as summarized in Table II. One quite noticeable characteristic is that the first-shell hyperfine interactions for Mn^{2+} in ZnSe and ZnTe

---

[26] A. Räuber and J. Schneider, Z. Naturforsch. **17a**, 266 (1962); R. S. Title, Phys. Rev. **131**, 623 (1963).

TABLE II. Reported values and upper limits for SHFS constants of S-state ions in II-VI compounds.

Ion	Parameter (10^{-4} cm^{-1})	ZnS(cubic)	ZnSe	ZnTe	CdS	CdSe	CdTe
Cr^+	$\lvert A_1 \rvert$	$\}\lesssim 2.2$	6.83	11.8			$\}\lesssim 10$[a]
	$\lvert B_1 \rvert$		4.41	21.83			
	$\lvert \bar{A}_2 \rvert$	~ 1.3	$\lesssim 0.5$				$\{5.82(\parallel)$[b] $5.62(\perp)$[b]
	$\lvert \bar{A}_3 \rvert$		1.65	3.54			
Mn^{2+}	$\lvert A_1 \rvert$		2.10	3.2			$\}\sim 10$
	$\lvert B_1 \rvert$		2.81	4.85			
	$\lvert \bar{A}_2 \rvert$	0.75[c]			2.6[d]	2.7[e]	2.6[f]
	$\lvert \bar{A}_3 \rvert$		0.44	1.14			
Fe^{3+}	$\lvert A_1 \rvert$		11.37	22[g]			
	$\lvert B_1 \rvert$		7.1	16[g]			
	$\lvert \bar{A}_2 \rvert$				$\lesssim 1.5$		
	$\lvert \bar{A}_3 \rvert$		$\lesssim 2.4$	$\lesssim 3$[g]			

[a] Based on analysis of Fig. 1 of Ref. 9.
[b] Reference 9.
[c] Reference 6.
[d] References 6–8.
[e] Reference 6.
[f] References 7, 8.
[g] Reference 25.

are less than those for either Cr^+ or Fe^{3+} in the same crystals by the ratio of 1:(3±1). Similarly, the third-shell interactions for Mn^{2+} are less than for Cr^+ and may be less than for Fe^{3+}, if the linewidth in these cases is primarily a result of unresolved SHFS with the third shells. In fact, the ratio is again close to 1:3. There appears to be an exception to this behavior in CdTe, where the Mn^{2+} first-shell interaction has been placed at about 10×10^{-4} cm^{-1} and the Cr^+ first-shell interaction is not larger than this value. The measurements on CdTe are much less reliable than those on the Zn compounds and should be given slight weighting in considering the systematic variations which may exist in the data.

An examination of the second-shell interaction in a given crystal for the three isoelectronic ions is more difficult because of the lack of data. The Cd interaction is less for Mn^{2+} than for Cr^+ in CdTe, and similarly the Zn^{67} interaction is less for Mn^{2+} than for Cr^+ in ZnS. However, the CdS:Fe^{3+} data show a still smaller Cd interaction for Fe^{3+} than for Mn^{2+}, which suggests a monotonic decrease in the second-shell metal interaction in going from Cr^+ to Fe^{3+}, in contrast to the minimum occurring at Mn^{2+} displayed by the first-shell nonmetal interaction.

The three Cd interactions are nearly identical for Mn^{2+} and the Zn^{67} interaction scales by about the ratio of the average gyromagnetic ratio for Cd^{111} and Cd^{113} to that of Zn^{67}. Similarly, the second-shell interactions for Cr^+ in CdTe and ZnS also scale according to the gyromagnetic ratios. Hence, the smallness of the Zn^{67} hyperfine interaction for Cr^+ in ZnSe seems to be an exception. This may not be the case, however, since the upper limit was established by determining the influence on the first- and third-shell Se^{77} SHFS of an isotropic Zn^{67} hyperfine interaction with no quadrupole effects included, whereas quadrupole effects appear to make significant contributions to the Zn^{67} SHFS for Cr^+ in ZnS. Hence the upper limit for ZnSe may be too low. The Se^{77} and Te^{125} hyperfine interactions are also approximately in the ratio of the gyromagnetic ratios, and the S^{33} upper limit for Cr^+ in ZnS is reduced by about this ratio from the value in ZnSe:Cr^+. The scaling by gyromagnetic ratio or nuclear g value is not

TABLE III. SHFS constants observed in present study.

Ion	Crystal	$\lvert A_1 \rvert$ (10^{-4} cm^{-1})	$\lvert B_1 \rvert$ (10^{-4} cm^{-1})	$\lvert \bar{A}_3 \rvert$ (10^{-4} cm^{-1})	a_1 (10^{-4} cm^{-1})	b_1 (10^{-4} cm^{-1})
Cr^+	ZnSe	6.83 ± 0.04	4.41 ± 0.03	1.65 ± 0.02	5.22	0.81
Cr^+	ZnTe	$11.8\ \pm 0.2$	21.83 ± 0.02	3.54 ± 0.04	18.49	-3.34[a]
Mn^{2+}	ZnSe	2.10 ± 0.08	2.81 ± 0.02	0.44 ± 0.03	2.57	-0.24[a]
Mn^{2+}	ZnTe	3.21 ± 0.15	4.85 ± 0.07	1.14 ± 0.03	4.29	-0.54[a]
Fe^{3+}	ZnSe	11.37 ± 0.08	7.14 ± 0.10	$\lesssim 2.4$	8.55	1.41
Fe^{3+}	ZnTe	22[b]	16[b]	$\lesssim 3$[b]	18	2
Cr^{2+}	ZnSe	$4.31G$[c]				
Fe^+	ZnTe	3.90 ± 0.05[d]				

[a] The negative signs for b_1 mean only that a_1 and b_1 differ in sign. No information on the sign of a_1 was obtained.
[b] Reference 25.
[c] Only the value for which the spin is quantized along the distortion axis can be measured. The value in 10^{-4} cm^{-1} is approximately that in gauss, but a precise reduction is not possible.
[d] For magnetic field along a ⟨100⟩ direction.

the obvious result of changing nuclei, since the contact hyperfine interaction should be proportional to $g_N|\psi(0)|^2$. The observations thus seem to imply that $|\psi(0)|^2$ for a given ion does not vary from crystal to crystal. Hence it appears that less wave function is required to explain the observation for heavy lattice neighbors than for the corresponding light one. This seems to run counter to the usual impressions as to the manner in which covalent bonding varies among the II-VI compounds.

In contrast to the results in ionic crystals, the SHFS with the neighbors in ZnSe and ZnTe is not always described by a hyperfine tensor with $|A|>|B|$. Both the Mn^{2+} cases and Cr^+ in ZnTe are exceptions. If the data for A_1 and B_1 are analyzed in terms of an isotropic contact interaction and an anisotropic dipolar interaction, then one has

$$\begin{aligned} A_1&=a_1+2b_1, \\ B_1&=a_1-b_1, \end{aligned} \tag{5}$$

where

$$\begin{aligned} a_1&=(8\pi/3)gg_N\beta\beta_N|\psi(0)|^2, \\ b_1&=(2/5)gg_N\beta\beta_N\langle 1/r^3\rangle. \end{aligned} \tag{6}$$

Two possibilities exist: Either A_1 and B_1 have the same or opposite signs. If like signs are assumed, $|a_1/b_1|$ is in the range from 5 to 10 for all six cases. If opposite signs are assumed, then $|a_1/b_1|$ is in the range from $\frac{1}{6}$ to 1. The ratio of a_1 to b_1 can be calculated in terms of the amount of ns and np neighbor wave function admixed into the d orbital. In this way, the case of like signs gives p-to-s ratios of between 2 and 4, very close to the value of 3 for the sp^3 hybridization utilized in the bonding in this coordination. If opposite signs are assumed, then there is 20 to 120 times as much p as s, a ratio which is not appealing on physical grounds. The slight evidence concerning the signs of A_1 and B_1 obtained from nuclear Zeeman effects in ZnSe:Cr^+ and ZnSe:Mn^{2+} also suggests that they are of like sign. Hence in Table III the data are analyzed making this assumption. Thus the results suggest somewhat more p than s character but a strong π-bonding contribution which is larger than the σ-bonding contribution in the three cases where a_1 and b_1 differ in sign.

These observations provide a fascinating basis for speculating on the theoretical interpretation. However, it appears that the only sure conclusion is that the treatment applied to ionic crystals will not fit more covalent crystals simply by increasing the magnitudes of the overlaps, admixtures, and other manifestations of covalency. Chen, Kikuchi, and Watanabe[27] have recently attempted a molecular-orbital treatment of Mn^{2+} in CdTe, and Chen[28] has made preliminary calculations for Cr^+, Mn^{2+}, and Fe^{3+} in ZnSe. It does not appear that such calculations can be refined to give the rather complex results reported and discussed here.

ACKNOWLEDGMENTS

The authors would like to thank R. Stinedurf for assistance in the experimental work, E. Jones and C. Ratliff for programming the SHFS reconstruction, J. Schneider for stimulating part of the early work, J. Chen for communicating his theoretical work in its early stages, and M. de Wit for helpful discussions at various phases of the work. We would particularly like to thank J. C. Hensel, who took additional data on ZnTe:Fe^{3+} so that we could obtain the Te superhyperfine splitting parameters.

---

[27] I. Chen, C. Kikuchi, and H. Watanabe, J. Chem. Phys. 42, 189 (1965).

[28] I. Chen (private communication).